6-DOF Force Sensing for the Master Tool Manipulator of the da Vinci Surgical System

David G. Black[1], Amir H. Hadi Hosseinabadi[1], Septimiu E. Salcudean, *Fellow, IEEE*

***Abstract*—We integrated a force/torque sensor into the wrist of the Master Tool Manipulator (MTM) of the da Vinci Standard Surgical system. The added sensor can be used to monitor the surgeon interaction forces and to improve the haptic experience. The proposed mechanical design is expected to have little effect on the surgeon's operative experience and is simple and inexpensive to implement. We also developed a software package that allows for seamless integration of the force sensor into the da Vinci Research Kit (dVRK) and the Robot Operating System (ROS). The complete mechanical and electrical modifications, as well as the software packages are discussed. Two example applications of impedance control at the MTM and joystick control of the PSM are presented to demonstrate the successful integration of the sensor into the MTM and the interface to the dVRK.**

***Keywords*—Haptics and Haptic Interfaces, Surgical Robotics - Laparoscopy, Force and Tactile Sensing, Telerobotics and Teleoperation, dVRK**

I. Introduction

CLOSE to 5,000 da Vinci systems are installed worldwide with more than 6 million procedures performed by the end of 2018 [3]. Due to the involved challenges in sensor design, safety concerns, and cost, no haptic feedback is yet provided in systems that are clinically in use [30]. While surgeons can use visual cues to develop an intuition of direct interaction with the tissue, haptic feedback is shown to improve task performance (quality and speed), decrease tissue trauma, and facilitate surgeons training in robotic MIS [10] [17]. However, its efficacy depends on the transparency level of the teleoperation system, the complexity level of the task - i.e. suturing, knot-tying, palpation, dissection, etc.- and the experience level of the surgeon [16]. According to Wagner et al. [4] [5], the lack of force feedback increases the average applied force magnitude on the tissue by 50% and the peak applied force by at least a factor of 2. Introducing force feedback decreased the rate of accidental tissue damage by a factor of 3.

However, the only experienced surgeons carrying out common surgical tasks using teleoperation are users of the da Vinci system. There is no prior work that integrates a 6-DOF force-sensor into the da Vinci master. This paper presents such a design, which does not change the da Vinci master kinematics and only marginally alters its dynamics.

Although adding haptic feedback can be effective, it presents challenges, both in sensing the forces and torques at the MTMs and PSMs, and in stable and transparent force reflection to the surgeon [2]. The transparency of a teleoperation system can be improved by adding information channels between the master and slave [31]. A four-channel interface where force and position data is exchanged between the master and slave is proven to provide the highest level of transparency [32]. Hashtrudi-Zaad et al. [11] showed that the same level of transparency can be achieved by closing the force feedback loop locally at the master or at the slave, thus reducing the number of communication channels. This approach, however, still requires force measurement at both the master and the slave manipulators.

While work has been reported on force sensing at the PSMs [6] [7] [8] [19], and four channel teleoperation in palpation and knot-tying tasks was addressed by Tavakoli and Patel [9], a four channel tele-operation interface has not been developed on a da Vinci system where the articulated wrist assemblies at the surgeon and patient side manipulators allow for dexterous tasks to be completed. Kamikawa et al. [33] presented a 3-DOF, force-controlled, tactile sensory substitution device at the finger grip of the MTM. The proposed design has a 3-axis force sensor at its base; however, its size significantly limits the motion envelope of the wrist assembly, reducing its maneuverability to perform dexterous tasks.

To acquire the force data, both sensor and model-based approaches were considered in prior work. Model-based approaches to force estimation include the use of motor currents [25], an observer [12], Kalman-Filter [13], or neural network [24]. In these methods, no additional sensors are required; however, unmodelled dynamics, (e.g. backlash and friction) and variations over time (e.g. cable tension), can lead to inaccuracies in force estimation. In contrast, force measurement techniques involve design of a custom sensor or integration of an off-the-shelf force sensor into the master manipulator.

Thus, instrumenting the master is the preferred method to develop a three or four channel [15] [11] teleoperation system. Additionally, force sensing at the master will enable novel studies in teleoperation, including the comparison of force sensing vs estimation.

The MTM instrumentation presents its own technical challenges, as described in this paper. Size and workspace restrictions are severely limiting, and the accurate capture of all 6

Manuscript received: Sept 10, 2019; Revised Dec 05, 2019; Accepted Jan 05, 2020.

This paper was recommended for publication by Editor Allison Okamura upon evaluation of the Associate Editor and Reviewers' comments. This paper was supported in part by NSERC and the Charles Laszlo Chair in Biomedical Engineering.

All authors are with the Robotics & Control Lab, Department of Electrical and Computer Engineering, University of British Columbia, Canada dgblack@ece.ubc.ca, ahhadi@ece.ubc.ca, tims@ece.ubc.ca

[1]The first and second authors contributed equally to this work and are co-first authors

Digital Object Identifier (DOI): see top of this page.

axes of force and torque, electrical and software integration, and increased inertia and friction are all important considerations. At the same time, the modifications to the original wrist design should be minimal in order to provide an interface as similar as possible to the original da Vinci system.

In section II the design considerations and objectives are discussed in more depth. Section III explains the mechanical design, section IV the electrical modifications, and section V the software architecture for sensor integration into the da Vinci Research Kit (dVRK). The last section details some applications that demonstrate the system's effectiveness.

II. System Design Objectives

The goal with the installation of a force sensor into the MTM is to accurately measure the forces and torques being applied by the surgeon, in all 6 axes, in real time, and without affecting the normal operation of the robot. In order to achieve this, there are a number of design requirements:

Sensor location:

- The sensor should be located as close as possible to the the finger grips to (1) minimize the effect of manipulator dynamics and (2) avoid large lever arms, which can saturate or break the sensor (see Fig. 4).
- The sensor must be installed in the load path, so it measures the full forces and torques being applied.
- The finger grips' position should remain unchanged. They are centred at the intersection of the wrist axes so moving them will introduce moment-arms, increase inertia, and change the surgeon's feel.

Mechanical:

- No parts should protrude into the workspace or affect the range of motion or operative experience. This is challenging because of the limited workspace and relatively large size of a force sensor with suitable range.
- The sensor and modified wrist should not add significant inertia or friction to the arm.

Electrical and Software:

- MTM sensors and motors should all function exactly as before
- The software should be integrated into ROS for real-time control with the dVRK.

Fig. 1. The original (left) and instrumented MTM (right), overlaid with the local coordinate system also seen in Fig. 3

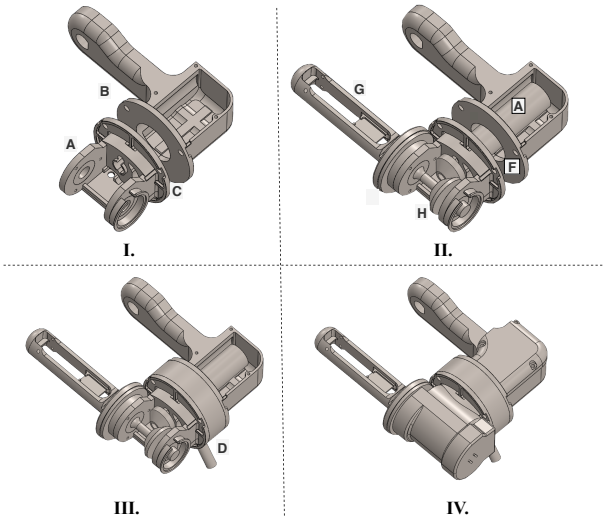

Fig. 2. The device CAD model in various states of assembly. I: Un-assembled yaw-link chassis in two parts (A,B) with mounting flange (C). II: Finger grips (G), motor (A) through hole (F), and bevel gears (H) added. III: ATI sensor (D) added. IV: Fully assembled.

III. Mechanical Design

The ideal position for the sensor is at the finger grips, closest to the surgeon interaction point. However, this would shift the position of the gripping location, cause interference issues, and/or force an alteration of the MTM kinematics. We therefore investigated different ATI force sensors, all of which provide resolutions higher than the human force perception threshold [26] [27] [28], to find one that satisfies the load and geometric constraints described later in this section (Fig. 4, Table I). An ATI F/T Nano43 sensor was chosen and integrated into the wrist yaw link as shown in Fig. 1. The wrist yaw link was broken into two components (A,B in Fig. 2.I) with connection interfaces (C) for the two faces of the ATI F/T sensor (D). The sensor does not increase the yaw link's length since the motor (E) and electrical connections pass through its centre hole (F). Thus, the finger grips (G) stay in exactly the same location as before, and the feel of the MTM is affected only by the small additional inertia. The sensor's orientation makes for an easy translation between sensor readings and actual user inputs. Proximal placement of the sensor to the finger grips keeps the lever arms short to avoid measurement saturation (Fig. 4).

This design was made with a focus on ease of manufacture. The designed parts that construct the wrist yaw link were 3D printed in Polylactic Acid (PLA). These parts are thicker than the original metal yaw link and have reinforcements to maintain rigidity. While the PLA 3D printing process is sufficient for research purposes, the manufacturing process could easily be changed (i.e. to molding, CNC machining, etc.) for production-quality components.

In designing the sensor interfaces, it was important to consider the transfer of wrenches (forces and torques) to the sensor. In the proposed design, 5 of the 6 DOFs are directly captured, and the axial torque about the finger grips can be

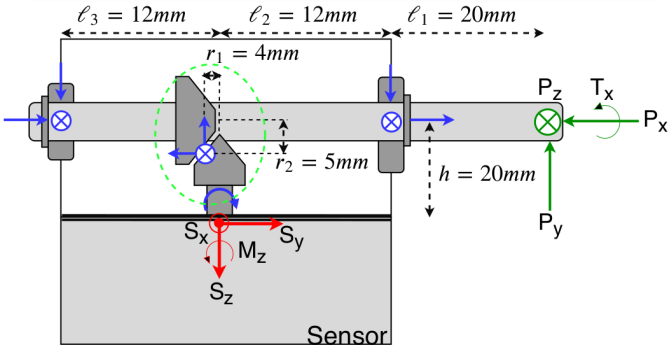

Fig. 3. Free body diagram of the MTM wrist assembly. Applied forces are green, intermediate reactions on the roll shaft are blue, and measured forces are red. Note, the directions of the applied forces and sensor forces are positive and thus indicate the respective coordinate systems. Also, most torques are left out of the diagram for clarity, and the bevel gears are circled in green.

recovered mathematically as explained below. The mapping from sensor measurement ($\vec{w}_s = [S_x, S_y, S_z, M_x, M_y, M_z]^T$) to applied wrench ($\vec{w}_f = [P_x, P_y, P_z, T_x, T_y, T_z]^T$) was geometrically derived from Fig. 3 and is shown in equation 1.

The axial torque about the finger grips, T_x, is transmitted through the bevel gears to the motor, as seen in Fig. 3. If the motor is off and not providing any resistance, the sensor will not pick up any torque. Conversely, if the motor resists all rotation, the sensor will measure the full applied torque. In normal operation, the system will be in some intermediate state and the torque is therefore not directly measured. However, as shown by equation 1, it is simple to calculate T_x from the measured S_x and M_y. Note, in equation 1, $\ell_{1+2} = \ell_1 + \ell_2$.

$$\vec{w}_f = \begin{bmatrix} 0 & 1 & 0 & 0 & 0 & 0 \\ 0 & 0 & -1 & 0 & 0 & 0 \\ -1 & 0 & 0 & 0 & 0 & 0 \\ \frac{r_2}{r_1}h & 0 & 0 & 0 & \frac{r_2}{r_1} & 0 \\ \ell_{1+2}+h & 0 & 0 & 0 & 1 & -1 \\ 0 & h & -\ell_{1+2} & -1 & 0 & 0 \end{bmatrix} \cdot \vec{w}_s \quad (1)$$

The da Vinci MTM is an impedance-type device, designed to require minimal forces to move when no haptic feedback is present [22] [14]. While the forces applied by the PSM at the tissue are at most $\pm 10N$ [16], force scaling is used to enhance the haptic experience for the surgeon [21]. Thus the maximum force that can be applied to the MTM had to be ascertained in order to choose a force sensor with sufficient load capacity. To this end, the MTM was locked in a stiff configuration, and forces were applied until the controller released the motors due to over-torque. A force sensor was placed on the finger grips, as in Fig. 5, and the wrench readings were transformed from the finger/gripper frame ($\vec{w}_f$) to the force sensor frame ($\vec{w}_s$) using the inverse of the matrix in equation 1. The resultant maximum values are shown in Table I.

TABLE I
MAXIMUM WRENCHES APPLIED TO MTM (UNITS OF N AND N.MM)

	F_x	F_y	F_z	T_x	T_y	T_z
Positive	7.4	8.8	4.5	170	185	442
Negative	-7.5	-4.4	-7.6	-191	-204	-223

The ideal operational range of the force sensor is a 6-

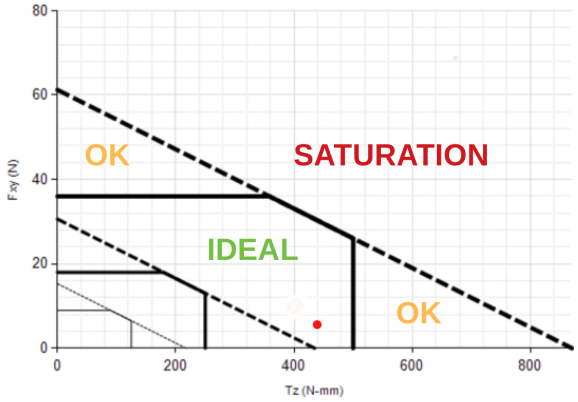

Fig. 4. Ideal range of ATI Nano43 F/T Sensor for torque about its axis, following equations 2 and 3 [23]. The maximum attainable value in the proposed design is indicated in red, at $T_z = 442N \cdot mm$, $F_{xy} = 8.8N$

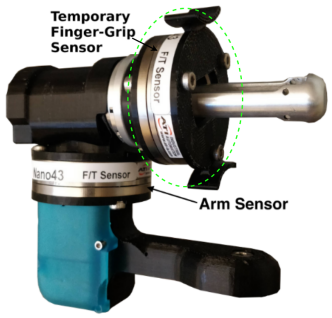

Fig. 5. Integration of a temporary second (finger grip) sensor for calibration and validation of the force/torque analysis and sensor accuracy

dimensional space of wrenches with an envelope defined by (in units of Newtons and Newton-millimeters):

$$\max|F_{x,y}| = \begin{cases} 36 & |T_z| < 400 \\ 62 - \frac{26}{400}|T_z| & 400 \leq |T_z| \leq 500 \end{cases} \quad (2)$$

$$\max|F_z| = \begin{cases} 36 & |T_{x,y}| < 310 \\ 72 - \frac{36}{310}T_{x,y} & 310 \leq |T_{x,y}| \leq 500 \end{cases} \quad (3)$$

It was found using the aforementioned maximum transformed wrenches that the measured wrenches fall within this space at all times, so the sensor never operates in the saturation region. Two dimensions of the region are displayed in Fig. 4, and the identified maximum values are within the ideal region.

A second sensor was temporarily attached to the finger grips to validate the force analysis and generate a mapping from applied force to measured force in the yaw link sensor. Using the setup in Fig. 5, a series of forces and torques was applied and measured by both the finger grip sensor and the yaw link sensor. With this data, a calibration matrix, C, was calculated such that $C\vec{w}_s = \vec{w}_f$. The 50000 measurements formed a matrix each for the finger-grip sensor (F) and arm sensor (S). The calibration was calculated as the least squares mapping from S to F:

$$C = \underset{C}{\operatorname{argmin}}||C \cdot S - F||_2^2 = FS^T(SS^T)^{-1} \quad (4)$$

After calibration, we ran a set of experiments to compare

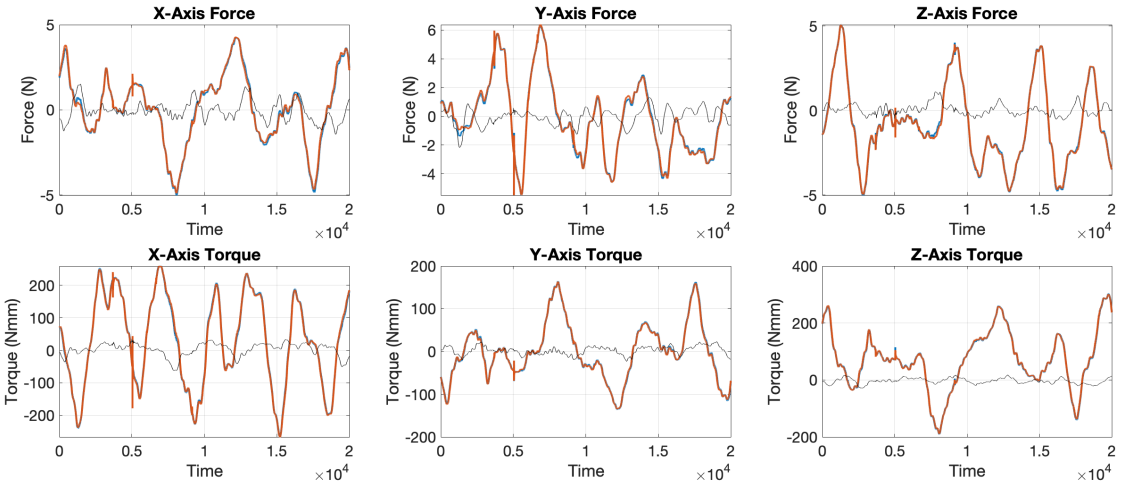

Fig. 6. Plots of the finger grip sensor reading (orange), transformed main sensor reading (blue), and 5×-magnified error (black) upon application of a series of wrenches. The listed axes are in the finger grips' coordinate frame. The transformation was performed using a calibration matrix derived using a separate measurement.

TABLE II
FORCE SENSOR RMS ERRORS

S_x	S_y	S_z	M_x	M_y	M_z
0.12N	0.13N	0.07N	2.1N.mm	4.4N.mm	2.1N.mm

TABLE III
IDENTIFIED DYNAMIC PARAMETERS

	I	B	F_c^+	F_c^-
Without Sensor	$2.5 \cdot 10^{-04}$	0.0028	-0.0021	-0.0021
With Sensor	$2.95 \cdot 10^{-04}$	0.0064	-0.0066	-0.0062

the directly measured forces with those generated by the yaw link sensor following the transformation by C (Fig. 6). The two matched up well in all axes, as shown by the RMS errors in Table II. The slightly larger error in M_y is due to some slipping of the calibration sensor on the finger grips. This affected not only the measured T_x, but also the P_z component of force because of the slightly varying orientation of the finger grip sensor with respect to the arm sensor. Further improvements to the remaining force/torque accuracies could be made by increasing the rigidity of the 3D-printed component. However, this was deemed undesirable considering the added inertia.

To determine how much the proposed design increases the wrist yaw linkage's inertia, a dynamics identification of the wrist yaw joint was carried out [34], both with the modified and original linkage attached. The identified parameters are shown in Table III, where I is the inertia about the joint axis ($kg \cdot m^2$), B is the viscous damping, and F_c^+ and F_c^- are the Coulomb friction values in the positive and negative directions, respectively. To test the effectiveness of the identification, a second set of velocity and torque data was obtained both with and without the sensor. The measured velocity and that calculated using the derived parameters was compared in both (Fig. 7), with acceptable tracking. The decrease in manufacturing precision due to 3D printing slightly increases the friction. More importantly, the described design increases the inertia by 18%.

We can gain further insight into the system by using the singular value decomposition, calculated in MATLAB. To quantify the effect of the sensor's positioning away from the point where the wrenches are applied, the condition number of

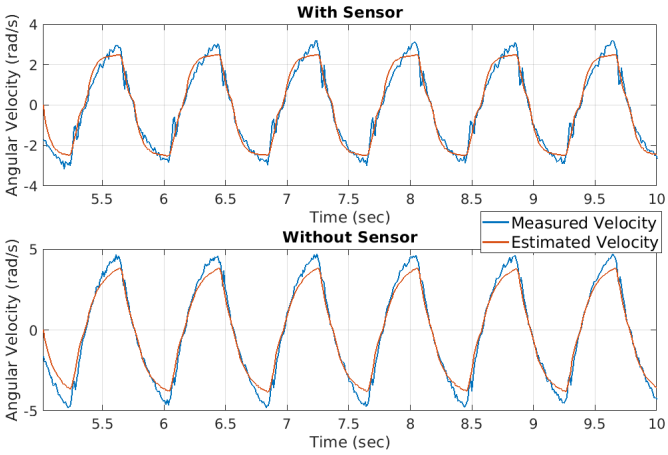

Fig. 7. Actual velocity (blue) and velocity predicted using the identified dynamic parameters (orange) of the wrist yaw linkage with and without sensor.

$C_{tot} = C \cdot C_{ATI}$ was calculated, where C_{ATI} is the voltage to force calibration matrix provided by ATI. The condition numbers of C_{tot} and C_{ATI} are 151 and 13, respectively. This indicates that the moment arm geometry between the wrench's actuation point and the sensor location causes a resolution loss of approximately 1 digit in addition to the existing loss due to C_{ATI}. The Nano43 force sensor reports 6×16 bit voltages with dynamic range of $\pm 10V$. Therefore, with the aforementioned resolution losses, the numerical resolution of the calibrated forces and moments due to round-off errors is 0.01. This is smaller than the ATI sensor's torque resolution

($0.1N \cdot mm$) and in the same order of magnitude as the force resolution ($0.007N$). Thus, although the measurement resolution is slightly decreased, it is still acceptable for a kinesthetic haptic feedback application [21]. The good fit of the curves validates the force analysis, and confirms that the wrist design provides high quality force/torque readings representative of the actual wrenches applied by the surgeon.

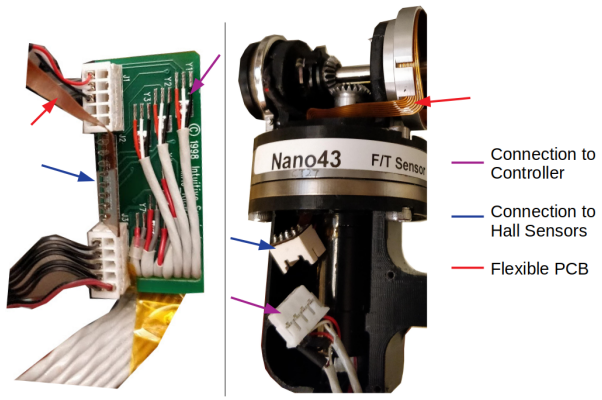

Fig. 8. The original electrical system (left) and updated one (right)

A. Electrical Design

While the electrical functionality of the instrumented wrist remains exactly the same as before, a number of changes had to be made to the connections and overall electrical setup to accommodate the mechanical alterations of the wrist. These are described briefly here, and in more detail in the web page linked in section VI

The primary change is a redesign of the wiring from the finger grip sensors. Two Hall effect sensors measure the angles of the finger grips; they interface through a flex circuit (red in Fig. 8) to a breakout board located close to the finger roll motor inside the wrist chassis. The breakout board and flex circuit had to be redesigned to fit inside the new yaw linkage. In the modified design, the flexible circuit terminates in a JST connector rather than in the breakout board (both blue in Fig. 8). This creates an easy, modular, space-efficient connector to the Hall effect sensors, motor, and encoders.

In addition to the finger grip wiring, the three wires going to the potentiometer of the roll motor were re-routed to go through the existing JST connector for the motor and encoder. A mating JST interface to the controller completes the setup.

These electrical alterations allow the sensor to be located as shown in Fig. 1 without affecting the functionality of the wrist. In fact, they make the whole setup more modular than it was before, as the JSTs can simply be unplugged, thus allowing the wrist to be removed completely from the rest of the arm, which was not previously an option.

B. Software Development

This section elaborates on the software architecture to access the ATI force/torque data in the dVRK for real-time control. The ATI F/T Nano43 sensors can interface with the host PC through a PCI-6220M DAQ card (National Instruments, Austin, Texas). Since the dVRK runs on a Linux operating system, we wrote a ROS package using Comedilib (comedi.org) in Python. The software reads the raw data from the force/torque sensors, processes it to resolve the force/torque values, and publishes the measurements to a ROS topic for other nodes to subscribe to.

This architecture ensures easy, instant compatibility with any dVRK software. While the overhead associated with ROS effectively limits the maximum sampling rate to 3kHz, this is fast enough for even the high-frequency control components of the dVRK system [20]. Two applications have been completed to demonstrate the ROS implementation efficacy (section IV).

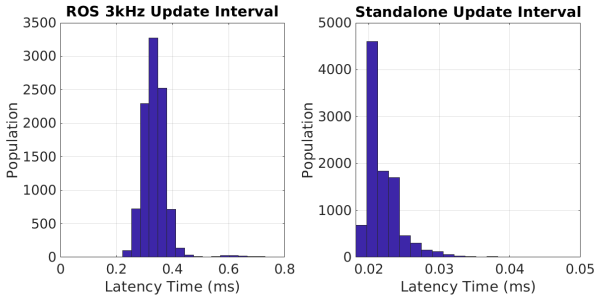

Fig. 9. Histograms showing the latencies (ms) in measuring 10,000 samples using ROS and the standalone software

However, if higher rates are needed, the Python script used to control the ROS node can also be imported directly into any control routine as a standalone Python package. This simple, user-friendly, object oriented interface foregoes the ROS overhead and is a thin Python wrapper over C++ code, so it can read and parse data at very high rates. The average latency time for the standalone package is $21.9\mu s$, as shown in Fig. 9. In this test, 10000 readings were taken from all 6 channels of the sensor, all the required modifications to the measured data were carried out, and each sample was both published to the ROS topic and passed directly to a control program using the standalone architecture. Ultimately, whichever software system is used, it either adequately meets or far exceeds the required speed for compatibility with the dVRK system [1].

In addition to reading and publishing quickly, the software has to perform some pre-processing on the raw measured data, as mentioned before. When launching the node, a single force measurement along with the orientation of the arm are saved as a bias measurement. Then, when data is read in from the sensor, it comes from all 6 channels and is combined into a 6-element vector of voltages. This vector is multiplied by the sensor-specific calibration matrix supplied by ATI to obtain a wrench. Concurrently, the software also stores the current orientation of the arm, with which the force is transformed to the base coordinate system, and the bias is subtracted. In this way, the measured force is always in the same coordinate system, irrespective of the MTM's current pose. Finally, the converted, calibrated, gravity-compensated

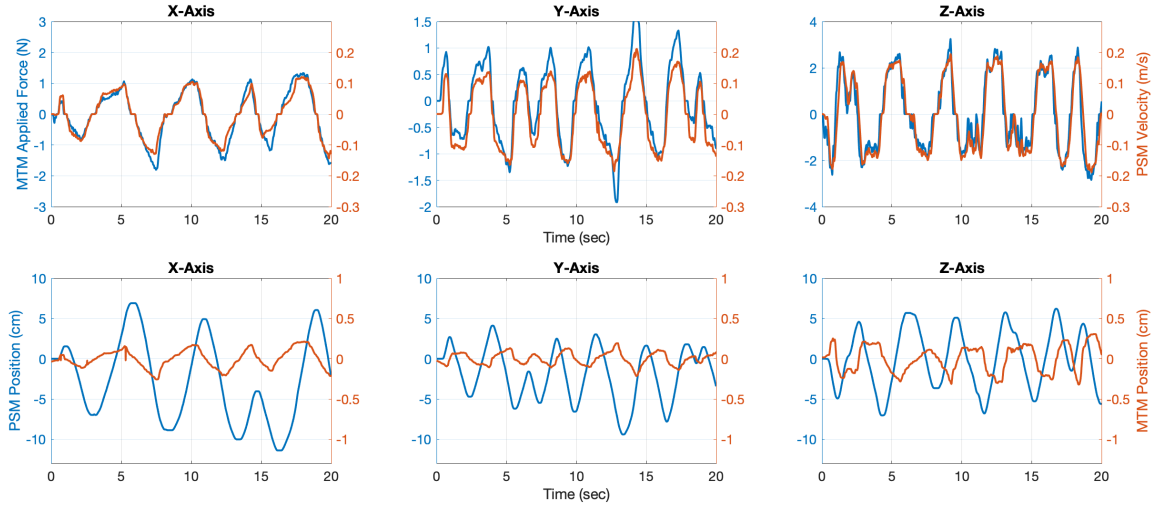

Fig. 10. Force-controlled joystick application- Top row: PSM velocity (orange) and applied force at the MTM (blue) in 3 axes. Bottom row: PSM position (blue) and MTM position (orange). The ratio of PSM to MTM motion amplitude is 23, 42, and 22 in x, y, and z respectively. This shows PSM velocity being controlled by MTM force with little to no movement in the MTM.

wrench is published to the ROS topic for use by other nodes.

IV. Applications

With the surgeon's applied wrench available in real time, a number of interesting applications are possible. These include, but are not limited to, improved teleoperation transparency, surgical skills assessment by monitoring operator interaction forces [18], learning from demonstration, improving the human-robot interface, and simplified gravity compensation. We demonstrate the successful integration of the instrument into the dVRK in two applications: PSM joystick control, and impedance control on the MTM. These applications show that the modified wrist design is completely functional, compatible with the dVRK, and provides high quality wrench data.

A. Force-Controlled Joystick

Currently, in the da Vinci system the PSM follows the position and orientation of the MTM. This means that if the PSM is far out of position, the surgeon has to repeatedly move the MTM extensively, press the foot pedal, return it to its original position, and repeat. Force control gives an alternative method of moving the PSM; instead of mimicking the position of the MTM, the PSM moves in the direction of the applied force with velocity proportional to the magnitude of the applied force. In this way, the MTM acts as a force-controlled joystick, and the slave can be moved across large distances without the user having to repeatedly use the foot pedal.

This is illustrated in Fig. 10. The top row of the figure shows the force applied by the user at the MTM and the velocity of the PSM, both measured simultaneously, while controlling the PSM by applying a random series of forces to the MTM. The bottom row shows the PSM position in blue and MTM position in orange, demonstrating that the PSM is indeed being force-controlled, not position-controlled.

Teleoperation is active only while the finger grips are closed. While open, the software re-biases the sensor. In this way, any force sensor drift is eliminated. Furthermore, to avoid moving into singularities found at either extremity of the PSM's range of motion, well outside the usual surgical workspace, and to increase intuitiveness by removing any coupling in the force measurements between the axes, we also tried controlling only one axis at a time. To cycle through the axes, one could simply release and re-grip the finger grips. In each mode, only forces in one direction were sent to the PSM as relative position commands. For example, in x-mode, only the forces in the x-axis were measured, and corresponding commands were sent only in the x-direction of the PSM. Releasing and re-gripping the finger grips switched the control to the y-direction, then the z-direction, then the gripper rotation.

Using this method, the joystick manipulation of the PSM was intuitive. Indeed, latency was low, at approximately $10.7ms$, and $70.7ms$ respectively in the y, and z axes, and negligible in the x axis, according to the normalized cross-correlation of the signals plotted in Fig. 10. As well, the RMS and maximum percent error between normalized velocity of the PSM and force applied to the MTM in the three axes were $E_{RMS} = (17.4\%,\ 12.4\%,\ 13.9\%)$, and $E_{max} = (33.9\%, 45.1\%, 64.3\%)$. The higher latency and velocity errors in z were due to high latency in the z-axis actuation of the PSM, not in the sensor or control system. Ultimately, the force control showed excellent promise for the sensor integration, including low latency measurements with small RMS errors in all DOFs.

B. Impedance Control

In a transparent haptic feedback system, force and velocity are measured at the tissue and relayed to the master. Since

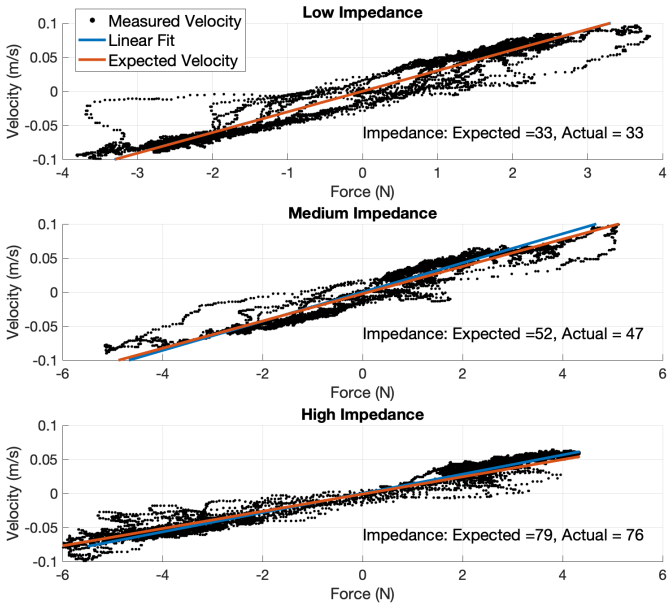

Fig. 11. MTM velocity vs. applied force in the y-direction at three impedance levels. Here 'impedance' is the ratio between velocity and force in the time domain, in units of $\frac{s}{kg}$

impedance is the ratio of force (F) to velocity (V) in the frequency domain, this data can be used to move the MTM with the calculated impedance of the PSM, thus giving the surgeon the impression of being in contact with the tissue.

To implement impedance control at the MTM, the surgeon's applied force at the MTM is measured, and a corresponding velocity command is given, proportional to the admittance-filtered force, i.e., $V = \frac{1}{Z}F$.

We used our force sensor to implement impedance control for various values of Z along the principal axes. Force and velocity of the MTM were then recorded under a series of random motions, and the actual impedance was calculated through a least squares linear fit. Fig. 11 shows results from the y-axis at two different impedance levels. The R-Squared values of the high, medium, and low impedance data sets are 0.966, 0.955, and 0.924 respectively, and the fitted slopes match the desired master impedance with errors less than 10%. Outlier data-points at the bottom-right and top-left of the plots are due to inertia of the arm caused by the use of the arm's full range of motion in the tests. This was especially apparent at low impedance, where the velocity was higher. This implementation was a simple, preliminary test to show the usefulness of the force sensing, and its compatibility with a four-channel teleoperation architecture. There are many more sophisticated approaches that compensate for dynamics that could be used [29].

V. Conclusion

The Master Tool Manipulator (MTM) of a standard da Vinci system was instrumented using an ATI Nano43 F/T sensor. The proposed design (1) requires minor modifications in the wrist yaw link, (2) does not change the location of the finger grips, (3) adds little inertia to the wrist yaw and pitch axes, and (4) does not limit the available wrist manipulation envelope. It is therefore expected that the sensor will not significantly change the surgeon's feel of interacting with the original MTM. A software interface was developed to provide user force/torque measurements to the dVRK control functions in real time, and with low latency. Finally, example applications of the sensed forces were presented to showcase successful integration of the instrumented MTM into the dVRK. The work presented in this paper is part of a larger-scope research effort in our group that is focused on improving the transparency of the tele-operation architecture, and the robot-user interface in da Vinci surgical systems. The high-fidelity tracking in the force control application, as well the accurate impedance, demonstrate that the sensor has been fully integrated into the dVRK and is ready to be used in a four channel teleoperation interface. The developments can potentially also be used in surgical skills assessment and research work on learning from demonstration.

VI. Software and Hardware Availability

In order to promote further research in this topic, we have made all of our work (software, CAD, etc.) available on GitHub. See the documentation there for much more detail, as well as instructions for use. https://bitbucket.org/RoboticsControlLab/davincimtmforcesensor/src

Acknowledgment

We would like to appreciatively recognize scholarship support from the NSERC Canada Graduate Scholarships-Doctoral program. Professor Salcudean gratefully acknowledges infrastructure support from CFI and funding support from NSERC and the Charles Laszlo Chair in Biomedical Engineering. The authors would also like to acknowledge Intuitive Surgical for providing the dVRK system used in this study and Dr. Peter Black MD for his insight and surgical perspective.

References

[1] P. Kazanzides, Z. Chen, A. Deguet, G.S. Fischer, R.H. Taylor, and S.P. DiMaio, "An Open-Source Research Kit for the da Vinci Surgical System," IEEE International Conference on Robotics & Automation (ICRA), 2014.

[2] A. Okamura, "Haptic feedback in robot-assisted minimally invasive surgery," Current opinion in Urology, Wolters Kluwer, 1st ed., vol. 19, pp.102-107, 2009.

[3] Intuitive Surgical Inc., "Investor Presentation Q3 2019," https://isrg.gcs-web.com/static-files/880bf027-e866-4c32-b910-5332467cd8dc

[4] C. Wagner, N. Stylopoulos, and R. Howe, "The role of force feedback in surgery: Analysis of blunt dissection," 10th Symposium on Haptic Interfaces for Virtual Environment and Teleoperator Systems, 2002.

[5] C. Wagner and R. Howe, "Force feedback benefit depends on experience in multiple degree of freedom robotic surgery task," IEEE Transactions on Robotics, 6th ed., vol. 23, pp.1235-1240, 2007.

[6] N. Zemiti, G. Morel, T. Ortmaier, and N. Bonnet, "Mechatronic Design of a New Robot for Force Control in Minimally Invasive Surgery," IEEE/ASME Transactions on Mechatroncs, 2nd ed., vol. 12, pp.143-153, 2007.

[7] B. Kuebler, U. Seibold, and G. Hirzinger, "Development of actuated and sensor integrated forceps for minimally invasive robotic surgery," The International Journal on Medical Robotics and Computer Assisted Surgery, 3rd ed., vol. 1, pp.96-107, 2006.

[8] T. Ortmaier, B. Deml, and B. Kuebler, "Robot assisted force feedback surgery," Advances in Telerobotics, Springer Tracts in Advanced Robotics (STAR), vol. 31, pp.341-358, Springer, 2007.

[9] M. Tavakoli and R.V. Patel, "Robotic suturing forces in the presence of haptic feedback and sensory substitution," Proceedings of 2005 IEEE Conference on Control Applications, pp.1-6, 2005.

[10] A. Talasaz, A.L. Trejos, and R.V. Patel, "Effect of force feedback on performance of robotics-assisted suturing," Proceedings of the IEEE RAS and EMBS International Conference on Biomedical Robotics and Biomechatronics, pp.823-828, 2012.

[11] K. Hashtrudi-Zaad, and S.E. Salcudean, "On the use of local force feedback for transparent teleoperation," Proceedings 1999 IEEE International Conference on Robotics and Automation (Cat. No.99CH36288C), vol. 3, pp.1863-1869, May 1999.

[12] P.J. Hacksel, and S.E. Salcudean, "Estimation of environment forces and rigid-body velocities using observers," Proceedings of the 1994 IEEE International Conference on Robotics and Automation, May 1994.

[13] Hu, J. and Xiong, R, "Contact force estimation for robot manipulator using semiparametric model and disturbance Kalman filter," IEEE Transactions on Industrial Electronics, 4th ed., vol. 65, pp.3365-3375, 2018.

[14] K. Hashtrudi-Zaad, and S.E. Salcudean, "Analysis of control architectures for teleoperation systems with impedance/admittance master and slave manipulators," The International Journal of Robotics Research, vol. 20, pp.419-445, 2001.

[15] A. Albakri, C. Liu, and P. Poignet, "Stability and performance analysis of three-channel teleoperation control architectures for medical applications," IEEE/RSJ International Conference on Intelligent Robots and Systems, 2013.

[16] A.L. Trejos, R.V. Patel, and M.D. Naish, "Force sensing and its application in minimally invasive surgery and therapy: a survey," Journal of Mechanical Engineering Science, vol. 224, pp.1435-1454, 2010.

[17] A. Talasaz, A.L. Trejos, and R.V. Patel, "The role of direct and visual force feedback in suturing using a 7-DOF dual-arm teleoperated system," IEEE Transactions on Haptics, 2nd ed., vol. 10, pp.276-287, 2017.

[18] A.L. Trejos, R.V. Patel, M.D. Naish, and M.C. Schlachta, "Design of a sensorized instrument for skills assessment and training in minimally invasive surgery," IEEE RAS & EMBS International Conference on Biomedical Robotics and Biomechatronics, 2008.

[19] A.H. Hadi Hosseinabadi, M. Honarvar, and S.E. Salcudean, "Optical force sensing in minimally invasive robotic surgery,", International Conference on Robotics and Automation (ICRA), 2019.

[20] Z. Chen, A. Deguet, R.H. Taylor, and P. Kazanzides, "Software architecture of the Da Vinci Research Kit," IEEE International Conference on Robotic Computing (IRC), 2017.

[21] L. Meli, C. Pacchierotti, and D. Prattichizzo, "Experimental evaluation of magnified haptic feedback for robot-assisted needle insertion and palpation," Int. J. Med. Robot. and Comput. Assist. Surg., vol. 13, no. 4, Dec. 2017.

[22] A. M. Okamura, L. N. Verner, T. Yamamoto, J. C. Gwilliam, and P. G. Griffiths, "Force feedback and sensory substitution for robot-assisted surgery," in Surgical Robotics: Systems Applications and Visions, Boston, MA: Springer US, 2011, pp. 419–448.

[23] ATI Industrial Automation, "F/T Sensor: Nano43", https://www.ati-ia.com/products/ft/ft_models.aspx?id=Nano43

[24] S. Abeywardena, Q. Yuan, A. Tzemanaki, E. Psomopoulou, L. Droukas, C. Melhuish, and S Dogramadzi, "Estimation of tool-tissue forces in robot-assisted minimally invasive surgery using neural networks," in Frontiers in Robotics and AI, vol. 6, pp. 56, 2019.

[25] B. Zhao, C. Nelson, "A sensorless haptic interface for robotic minimally invasive surgery," Thesis, University of Nebraska, 2015.

[26] E. Mesa-Munera, J.F. Ramirez-Salazar, P. Boulanger, W.F. Bischof, and J.W. Branch, "Estimation of vibration and force stimulus thresholds for haptic guidance in MIS training," Rev. Biomed. Eng., Vol.5, No.10, 2011.

[27] B. Wu, R. Klatzky, R. Lee, V. Shivaprabhu, J. Galeotti, M. Siegel, J.S. Schuman, R. Hollis, and G. Stetten, "Psychophysical evaluation of haptic perception under augmentation by a handheld device," Human Factors and Ergonomics Society, Vol. 57, No. 3, pp. 523-537, 2014.

[28] M. Zhou, J. Perreault, S.D. Schwaitzberg, and C.G.L. Cao, "Force perception threshold varies with experience in minimally invasive surgery," IEEE International Conference on Systems, Man and Cybernetics, 2007.

[29] A. Munawar and G. Fischer, "A surgical robot teleoperation framework for providing haptic feedback incorporating virtual environment-based guidance," Frontiers in Robotics and AI, Vol. 3, pp. 27, 2016.

[30] A. Saracino, A. Deguet, F. Staderini, M.N. Boushaki, F. Cianchi, A. Menciassi, and E. Sinibaldi,"Haptic feedback in the da Vinci Research Kit (dVRK): A user study based on grasping, palpation, and incision tasks," International Journal of Medical Robotics, Vol. 15, No. 4, 2019.

[31] A. Aziminejad, M. Tavakoli, R.V. Patel, and M. Moallem, "Transparent time-delayed bilateral teleoperation using wave variables," IEEE Transactions on Control Systems Technology, Vol. 16, No. 3, 2008.

[32] D.A. Lawrence, "Stability and transparency in bilateral teleoperation," IEEE Transactions on Robotics and Automation, Vol. 9, No. 5, 1993.

[33] Y. Kamikawa, N. Enayati, A.M. Okamura, "Magnified force sensory substitution for telemanipulation via force-controlled skin deformation," IEEE International Conference on Robotics and Automation, 2018.

[34] K. Erkorkmaaz and Y. Altintas, "High speed CNC system design. Part II modeling and identification of feed drives," Int. Journal of Machine Tools and Manufacture, Vol. 41, pp. 1487-1509, 2001.